

RESEARCH ARTICLE | MAY 17 2024

Graphics processing unit/artificial neural network-accelerated large-eddy simulation of swirling premixed flames

Min Zhang (张敏)  ; Runze Mao (毛润泽); Han Li (李晗); Zhenhua An (安振华)  ; Zhi X. Chen (陈帜)  



Physics of Fluids 36, 055147 (2024)

<https://doi.org/10.1063/5.0202321>



View
Online



Export
Citation



Physics of Fluids

Special Topic:
Selected Papers from the 2023 Non-Newtonian
Fluid Mechanics Symposium in China

Submit Today



Graphics processing unit/artificial neural network-accelerated large-eddy simulation of swirling premixed flames

Cite as: Phys. Fluids **36**, 055147 (2024); doi: [10.1063/5.0202321](https://doi.org/10.1063/5.0202321)

Submitted: 3 February 2024 · Accepted: 3 May 2024 ·

Published Online: 17 May 2024



View Online



Export Citation



CrossMark

Min Zhang (张敏)^{1,2} Runze Mao (毛润泽)¹, Han Li (李晗)^{1,2}, Zhenhua An (安振华)³ and Zhi X. Chen (陈帆)^{1,2,a}

AFFILIATIONS

¹State Key Laboratory of Turbulence and Complex Systems, College of Engineering, Peking University, Beijing 100871, China

²AI for Science Institute (AISI), Beijing 100080, China

³State Key Laboratory of Multiphase Flow in Power Engineering, Xi'an Jiaotong University, Xi'an 710049 China

^aAuthor to whom correspondence should be addressed: chenzhi@pku.edu.cn

ABSTRACT

Within the scope of reacting flow simulations, the real-time direct integration (DI) of stiff ordinary differential equations for the computation of chemical kinetics stands as the primary demand on computational resources. Meanwhile, as the number of transport equations that need to be solved increases, the computational cost grows more substantially, particularly for those combustion models involving direct coupling of chemistry and flow such as the transported probability density function model. In the current study, an integrated graphics processing unit-artificial neural network (GPU-ANN) framework is introduced to comply with heavy computational costs while maintaining high fidelity. Within this framework, a GPU-based solver is employed to solve partial differential equations and compute thermal and transport properties, and an ANN is utilized to replace the calculation of reaction rates. Large eddy simulations of two swirling flames provide a robust validation, affirming and extending the GPU-ANN approach's applicability to challenging scenarios. The simulation results demonstrate a strong correlation in the macro flame structure and statistical characteristics between the GPU-ANN approach and the traditional central processing unit (CPU)-based solver with DI. This comparison indicates that the GPU-ANN approach is capable of attaining the same degree of precision as the conventional CPU-DI solver, even in more complex scenarios. In addition, the overall speed-up factor for the GPU-ANN approach is over two orders of magnitude. This study establishes the potential groundwork for widespread application of the proposed GPU-ANN approach in combustion simulations, addressing various and complex scenarios based on detailed chemistry, while significantly reducing computational costs.

Published under an exclusive license by AIP Publishing. <https://doi.org/10.1063/5.0202321>

15 July 2024 11:46:55

I. INTRODUCTION

Large eddy simulation (LES), known for its proficient modeling of the interaction between turbulence and chemistry, is commonly used to simulate canonical flames. Recently, LES has been increasingly applied to real industrial combustors. For instance, Poinsot¹ performed LES to predict the combustion instabilities in real engines. Mueller and Pitsch² applied LES to simulate soot evolution in a Pratt & Whitney aircraft gas turbine combustor. However, applying LES to high-fidelity simulations of turbulent flames under realistic conditions still suffers from heavy computational costs.³ In the realm of reacting flow simulations, it is widely acknowledged that the computation of chemical kinetics through real-time direct integration (DI) of stiff ordinary differential equations (ODE) is the predominant consumer of computational resources. To illustrate, in cases where the reaction involves

more than 50 species, the chemical kinetics component can account for approximately 90% of the total computational effort.⁴

In addressing the aforementioned challenge, significant endeavors have been undertaken to reduce the computational demands of processing chemical kinetics by streamlining the real-time solution of ODE. One of the most important options for decreasing the computational burden associated with the DI of ODE is to utilize various forms of tabulation methods that leverage a pre-computed database of reaction source terms.^{5,6} Among these approaches, flamelet-generated manifold (FGM) is a popular technique that uses several variables (such as mixture fraction and progress variable) to look up the pre-computed table.⁷ The FGM has been widely implemented in the turbulent flame.^{8–10} Mueller,⁹ for example, has developed a manifold-based combustion model that effectively describes arbitrary multi-modal

combustion processes with unity Lewis numbers and with differential diffusion. It should be noted that more look-up variables are required to tackle complicated conditions. This leads to a significant increase in memory requirements. To minimize memory usage and enable the use of large-scale mechanisms, two innovative methods have been introduced: intrinsic low-dimensional manifold (ILDM)¹¹ and *in situ* adaptive tabulation (ISAT),¹² with the latter involving the dynamic updating of chemistry tabulation throughout the simulation. Recently, Newale *et al.*¹⁰ combined the pre-partitioned adaptive chemistry (PPAC) methodology with *in situ* adaptive tabulation (ISAT) to further reduce the computational cost. Nevertheless, tabulation techniques ease the computational load while potentially compromising the accuracy of physical fidelity. For instance, species that undergo slower chemical reactions, such as acetylene (C_2H_2) and nitrogen dioxide (NO), require a longer duration to adjust to changes in the dissipation rate, thereby resulting in an underestimation of their concentration levels.¹³ In addition, the underestimations of C_2H_2 and NO consequently lead to prediction errors of soot and nitrogen oxides (NOx). As a result, the aforementioned tabulation methods may not be an effective option in certain scenarios.

It is well known that employing finite rate chemistry (FRC) in combustion modeling typically results in more precise reaction processes without limiting the scenarios. Recently, there has been a fast-paced growth in the field of artificial intelligence (AI), mainly in the area called machine learning (ML). This growth has opened up fresh views on speeding up detailed FRC while still maintaining high accuracy. A common approach to accelerate FRC is to apply a neural network as a substitute for the DI of the stiff ODE.^{14,15} Christo *et al.*¹⁶ employed a single artificial neural network (ANN) to tabulate simple mechanisms, specifically the three- and four-step chemical systems involved in combustion, showing the potential of ANN to substitute the ODE integration. In the prior study by Brown *et al.*,¹⁷ parallel residual networks (ResNets) were employed to address the stiff ODE dictated by the chemically reacting flows. This was executed using a simplified hydrogen H₂-air reaction model that encompassed 8 species and 18 reactions.¹⁸ Recently, several feature reduction techniques coupled with ANN have been employed when large data sets were involved. For instance, Blasco *et al.*^{19,20} partitioned the composition space into multiple subdomains within thermochemical space (such as mixture fraction or temperature) using the automatic partitioning technique known as self-organizing map (SOM). Each subdomain was then fitted with an individual ANN. In another study,^{21,22} principal component analysis (PCA) was combined with an ANN to enhance the size-reduction capabilities of PCA and address the inefficiencies of the statistic-based nonlinear regression model in fitting highly nonlinear datasets. Additionally, Castellanos *et al.*²³ proposed time-lag autoencoders, which enhance the reconstruction of the thermochemical process's temporal progression. However, this study did not employ an ANN model as a substitute for the ODE integrator. More recently, Goswami *et al.*²⁴ have successfully integrated an autoencoder into the DeepONet frameworks, demonstrating exceptional accuracy for species that evolve over considerably shorter time scales.

In practice, the primary challenge when using the ANN to accelerate the direct integration of ODEs lies in the ANN that can generalize across a wide range of realistic combustion scenarios. To achieve such generalization capabilities, the crucial step is to sample training data comprehensively. An *et al.*²⁵ trained an ANN using the training

data collected from a Reynolds-averaged Navier-Stokes (RANS) simulation and then applied it to the LES case. High-precision results, in terms of ignition quenching and mass fraction prediction, can be achieved in comparison to a conventional ODE integrator. Weng *et al.*²⁶ sampled data from the LES case and extended the concept of Fourier Neural Operator (FNO) to learn stiff chemical kinetics. It is apparent that sampling training data from a specified RANS/LES case limits the generalization capabilities of the trained ANN. In contrast to sample training data from the RANS case, a multi-scale sampling method has been introduced for sampling data in several studies.^{27,28} For instance, Zhang *et al.*²⁷ used the multi-scale sampling method to collect training data across the full composition space, demonstrating strong generalization capability for a range of flame configurations. However, training costs rise significantly with more than 5×10^6 samples and upward of 1.6×10^6 model parameters. Recently, Readshaw *et al.*²⁹ and Ding *et al.*³⁰ proposed a hybrid method, known as HFRD-MMLP (Hybrid Flamelet/Random Data and Multiple Multilayer Perceptrons), to simulate the Cambridge stratified flame. The same technique was applied to various fuels [dimethyl ether and blends of methane (CH₄) and H₂] and flame configurations (Sandia flame D and the Sydney bluff-body flame), demonstrating exceptional accuracy relative to the direct integration of ODE and robust generalization capability.^{31,32} It is widely recognized that as the number of transport equations to be solved increases, the computational cost becomes more significant, thereby diminishing the overall acceleration factor despite the use of ANN to expedite the integration of ODE. This phenomenon is illustrated in the study by Readshaw *et al.*,²⁹ where the reaction source term is reduced by a factor of 14, yet the overall acceleration factor is only about 4.

Graphics processing units (GPUs), originally engineered for the highly parallel task of rendering graphics, can greatly enhance the speed of computational fluid dynamics (CFD) simulations.³³⁻³⁶ Le *et al.*³⁷ were at the forefront in developing one of the initial GPU solvers for reactive flows. This solver utilizes an explicit finite volume method (FVM) for solving the fluid equations and implements a first-order implicit approach for handling the chemical kinetics terms. Their research has shown that it can achieve a speedup of up to 40 times when compared to running on a single CPU thread. Pérez *et al.*³³ carried out direct numerical simulations (DNS) of reacting flows with detailed chemistry using many-core/GPU acceleration with the KAUST adaptive reacting flows solver (KARFS). Levesque *et al.*³⁸ accomplished the adaptation of Sandia National Laboratories' DNS code, S3D, for GPU environments. This was achieved by leveraging OpenACC directives in combination with message passing interface (MPI) and OpenMP, facilitating architecture-independent, multi-tier parallelism. Recently, Bielawski *et al.*³⁴ developed a high-speed reacting flow GPU solver within the framework of OpenFOAM, which showcased remarkable parallel scalability across thousands of GPUs. Henry de Frahan *et al.*³⁶ introduced PeleC, an adaptive mesh refinement solver for compressible reacting flows. They demonstrated PeleC's capability for exascale computing with a simulation of 160×10^9 cells and showed that it can weakly scale to fully utilize 100% of the Summit supercomputer's resources.

Although the acceleration of CFD using GPUs and the substitution of the ODE solver with an ANN model have been widely explored in separate efforts, integrating an ANN model into a GPU-based CFD solver is expected to further reduce the aforementioned bottleneck associated with computational costs while maintaining high fidelity.

To achieve this, a GPU-AI approach is proposed and employed to simulate the Xi'an Jiao Tong University (XJTU) swirling flame³⁹ and Cambridge high-swirling stratified flame.⁴⁰ The LES of these two swirling flames serves as a robust validation to affirm and extend the proposed GPU-AI approach to complicated turbulent conditions. To the best of the authors' knowledge, simulations conducted using an integrated GPU-ANN approach have rarely been reported, especially not for laboratory-scale turbulent flames. This could constitute a substantial and unique novel contribution to promoting ANN and GPU techniques to be widely used in the combustion community.

The remainder of this paper is structured as follows: the integrated GPU-AI framework including GPU acceleration, training data, and ANN model is briefly introduced in Sec. II. The evaluation of the integrated GPU-ANN approach is performed by comparing the macro flame structure of the XJTU swirling flame and detailed statistical characteristics of the Cambridge Stratified flame in Secs. III and IV, respectively. The computational saving is analyzed in Sec. V. Finally, concluding remarks are provided in Sec. VI.

II. INTEGRATED GPU-AI FRAMEWORK

In the authors' previous work,⁴¹ the solvers are central processing unit (CPU)-based in the developed open-source code, DeepFlame,⁴¹ which enhances its performance by integrating the robust fluid dynamics functionalities of OpenFOAM,⁴² the specialized thermochemical analysis capabilities of Cantera, and the sophisticated machine learning algorithms provided by PyTorch.⁴³ It is important to highlight that DeepFlame is not a distinct methodology; instead, it serves as an open-source platform that allows researchers to implement their own ANN models, acceleration techniques, and simulation scenarios. As an example, the present study has successfully incorporated an integrated GPU-AI framework. Details on this GPU-AI framework are described later.

A. GPU acceleration framework

Figure 1 shows the framework of GPU acceleration for dfLowMachFoam, which is one of the solvers for DeepFlame open-source code. As illustrated in Fig. 1, only the initializing data at the first step and writing out the simulation results are carried out on CPU to avoid the CPU-GPU memory copy overhead. The computational process executed on GPU mainly can be categorized into three parts:

- **Solve partial differential equations (PDEs).** Fully implicit pressure-based PDEs are solved for mass, momentum, species, energy, and pressure using the FVM. The sparse matrix, which represents a linear system post-discretization in the implicit FVM, has its storage format transformed from the lower-diagonal-upper (LDU) to the compressed sparse row (CSR) format within the current GPU framework. The implicit discretization is executed with compute unified device architecture (CUDA) kernel functions to guarantee precise management of threads and memory. Subsequently, the Algebraic Multigrid Solver (AmgX) library⁴⁴ produced by NVIDIA is utilized to solve the linear system.
- **Infer chemical source terms with ANN.** The conventional DI of ODE is substituted by ANN inference. The ANN-related operations are implemented based on the libTorch library.⁴⁵ To enhance computational efficiency during the inference procedure, the model adopts the half-precision floating-point format.

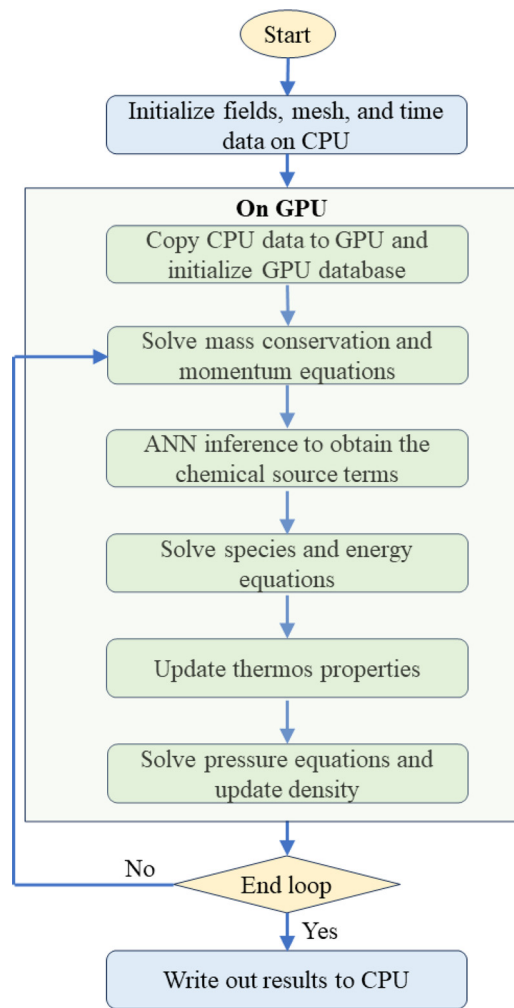


FIG. 1. Flow chart of the integrated GPU-AI framework.

Furthermore, a dynamic inference batch size is employed to mitigate the GPU memory footprint.

- **Update thermal and transport properties.** The update operations for thermal and transport properties, involving Newton's method and high-order temperature polynomials, are conducted through CUDA functions.

Additionally, for direct GPU communication, the NVIDIA collective communication library (NCCL) is employed instead of the conventional message-passing interface (MPI) approach to achieve multi-processor parallelism. Moreover, various optimizations have been performed to increase computational performance and minimize the GPU memory footprint. The relevant code implementation can be found on our GitHub site.⁴⁶

B. Training data and DNN model generation

The instantaneous reaction rates of a given mechanism, determined by local species concentration (y_i), temperature (T), and pressure (p), can be solved by the following systems of ODEs:

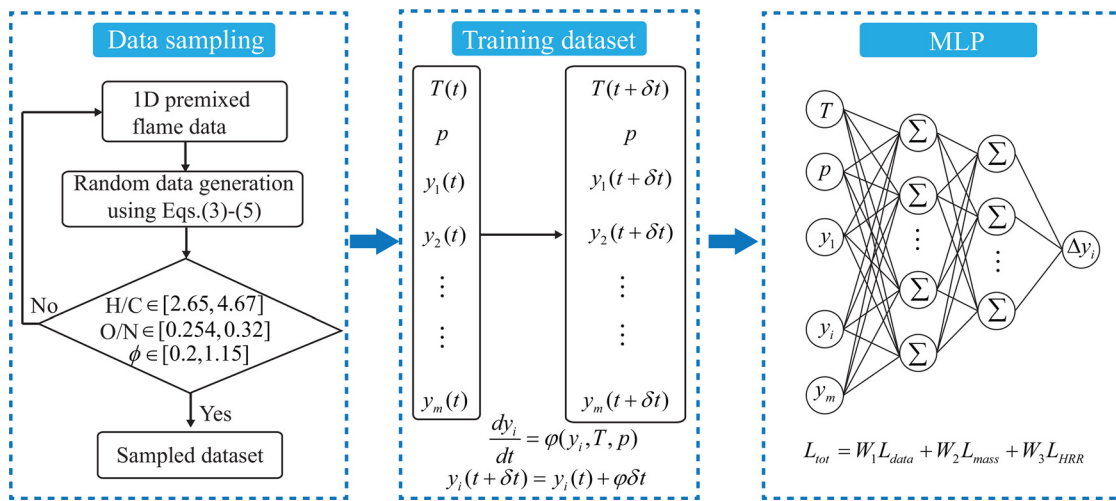


FIG. 2. Scheme of the process of training data and ANN model generation.

$$\dot{\omega}_k = \frac{dy_i}{dt} = \varphi(y_i, T, p). \quad (1)$$

Given a specific initial composition, the numerical integration of Eq. (1) over a time step, δt , produces an input–output pair as follows:

$$[T(t), p, y_i(t)] \Rightarrow [T(t + \delta t), p, y_i(t + \delta t)]. \quad (2)$$

The core principle behind substituting ANN for reaction rate calculations lies in the fact that the procedure, referenced in Eq. (2), can be approximated through a non-linear optimization process, widely known as training. The hybrid flamelet/random data (HFRD) methodology proposed by Readshaw *et al.*²⁹ and Ding *et al.*³⁰ is employed in the present study. Only a brief training data generation procedure and its new developments are presented here. Figure 2 illustrates a brief description of the procedures for employing ANN methodology in the present study, which consists of the following three steps:

- **Sample and generate random data from flamelet data.** The random data generation process can increase the generality of the training data and thus make the ANN model more robust to their own prediction errors. This step primarily involves sampling data from flamelet simulations and generating random data points based on the sampled flamelet data. The detailed procedures are described here. First, initial data are sourced from one-dimensional (1D) premixed flame simulations, which are conducted using the CPU-based dfLowMachFoam solver in DeepFlame.⁴¹ The chemical mechanism used for the simulation is DRM19, which consists of 20 species and 85 reactions.⁴⁷ The detailed configurations of 1D premixed flame are given in Table I. Subsequently, the dataset derived from the 1D simulations provides the basis for random data generation. For every composition within the flamelet dataset, a new random composition is generated through the following procedures:

$$T' = T + \alpha\gamma(T_{\max} - T_{\min}), \quad (3)$$

$$p' = p + \beta\gamma(p_{\max} - p_{\min}), \quad (4)$$

TABLE I. Configurations of 1D premixed flame.

Parameters	Value
Number of flames	62
Equivalence ratio range	0.45–1.10
Grid nodes	500
Initial temperature	300 K
Pressure	1 bar
Simulation time duration	0.005 s
Min reactive temperature	500 K

$$y'_{N_2} = y_{N_2} + \alpha\gamma(y_{N_2,\max} - y_{N_2,\min}), \quad (5)$$

$$y'_j = y_j^{(1+\theta\gamma)}, \quad (6)$$

where the parameters α , β , and θ are set to 0.125, 10.0, and 0.1, respectively. The same values of α and θ used in the study by Readshaw *et al.*²⁹ were adopted in the present study. The value of $\beta = 10$ is employed to reasonably cover the varying pressures in the flamelet data. γ is random number within $[-1,1]$ with uniform distribution. Although it is feasible to assume a fixed pressure in two swirling flames for the present study, the pressure is included as one of the inputs for the ANN model as compared to the study by Readshaw *et al.*²⁹ This allows the current ANN framework to be applied to a broader range of conditions involving pressure changes in the future. Moreover, the randomly generated data, following the mentioned method, should adhere to various specified constraints. Initially, the mass fractions of species must collectively sum to unity. Additionally, the molar element ratio and equivalence ratio of each composition state in the random dataset must possess appropriate values. Specifically, $H/C \in [2.65, 4.67]$, $O/N \in [0.254, 0.320]$, and equivalence ratio $\in [0.20, 1.15]$ are used in the present study. Figure 3 shows a comparison between flamelet data, random data, random data

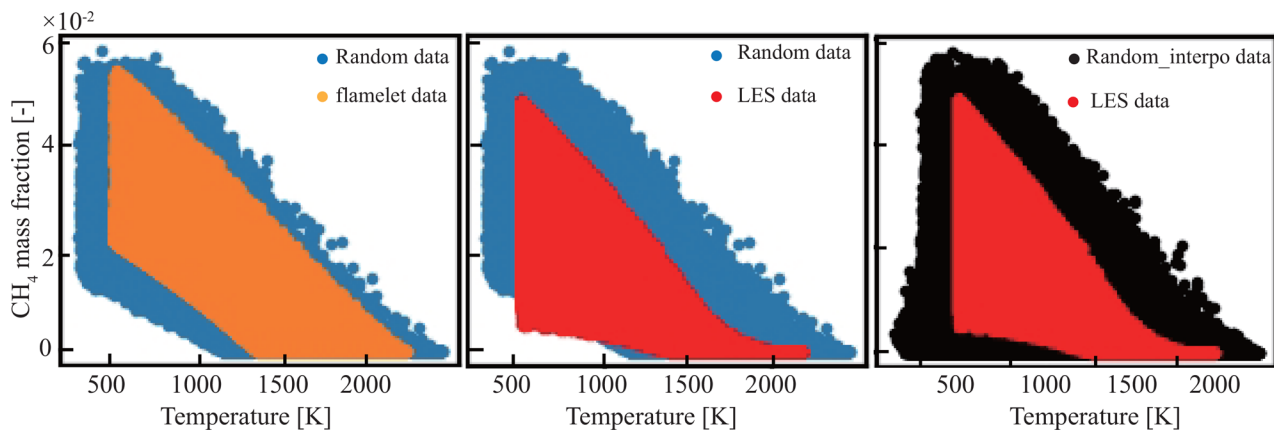


FIG. 3. Comparison of scatter plots between the flamelet dataset, random dataset, random data after interpolation, and LES data collected from direct integration of Cambridge swirling flame in $T\text{-CH}_4$ space.

with interpolation, and data collected from the LES simulation of Cambridge stratified flame. It is clear that the flamelet data after random generation almost cover the LES data. However, the mixing of extremely lean reactants with high-temperature products, which primarily occurs due to entrainment from large eddy structures, cannot be accounted for, as shown in Fig. 3(b). As a result, linear interpolation is used for all species, bridging the equilibrium compositions of the lowest equivalence ratio and the ambient air compositions, as illustrated in Fig. 3(c).

- **Generate training data.** After generating the random dataset, each composition within it is processed using the CVODE integrator in Cantera⁴⁸ for a time step of $1\ \mu\text{s}$ to obtain the target output. Adopting a fixed time step is a commonly used approach for ANN replacing ODE integration.²⁹ Training an ANN model suitable for varying time steps will be future work. In this study, a total of 518 000 input-output pairs are produced to form the final training dataset.
- **ANN training using multilayer perceptrons (MLP).** The MLP approach is employed in the present study. According to Eq. (1), the input layers of the MLP can be represented as $\varphi(t) = \{T(t), p(t), \mathcal{F}(Y(t))\}$. The output layers represent the variation in the mass fractions of species across a specified time interval, represented as $\mathbf{u}^*(t) = Y(t + \Delta t) - Y(t)$. Since the different species exhibit disparate orders of magnitude in thermochemical phase space throughout the evolution of the chemical system, the Box-Cox transformation (BCT), proposed by Box and Cox⁴⁹ and introduced for preprocess of training data in the study by Zhang *et al.*,²⁷ is employed here to represent multi-scale data by $O(1)$ quantity and avoid the singularity arising from the log transformation when the data approach zero, such that

$$f(x) = \begin{cases} \frac{x^{\lambda-1}}{\lambda}, & \text{if } x > 0 \\ \log(x), & \text{if } x \leq 0 \end{cases} \quad (7)$$

where $\lambda = 0.1$ is adopted in the present study. The mass fraction of the chemical species within $[0, 1]$ is mapped to $[-1/\lambda, 0]$ after the BCT. Training and prediction are individually performed for

each species' mass fraction to ensure high accuracy. The architecture of each MLP similar to the study by Zhang *et al.*²⁷ includes hidden layers consisting of 1600, 800, and 400 perceptrons, respectively. The network utilizes the Gaussian error linear unit (GELU) as its activation function, and hyperparameter optimization is carried out using the Adam algorithm. Training the ANN involves evaluating a loss function that compares its predictions against the training data, which represents the numerically integrated solution of the complete chemical system:

$$\mathcal{L}_{\text{data}} = \frac{1}{N} \sum_{i=1}^N (\mathbf{Y}_i^*(t + \Delta t) - \mathbf{Y}_i(t + \Delta t))^2. \quad (8)$$

Since the full thermochemical space obeys the conservation of the species mass fractions during the reaction as the solution vector evolves, the loss corresponding to this physical constraint is expressed as follows:

$$\mathcal{L}_{\text{mass}} = \left| \sum_{i=1}^N \mathbf{Y}_i^*(t + \Delta t) - 1 \right|. \quad (9)$$

With the consideration of the heat release rate (HRR), the additional loss is described as follows:

$$\mathcal{L}_{\text{HRR}} = (\mathbf{HRR}^*(t + \Delta t) - \mathbf{HRR}(t + \Delta t))^2. \quad (10)$$

The total loss function for the ANN takes the form

$$\mathcal{L}_{\text{tot}} = W_1 \mathcal{L}_{\text{data}} + W_2 \mathcal{L}_{\text{mass}} + W_3 \mathcal{L}_{\text{HRR}}, \quad (11)$$

where the weights W_1 , W_2 , and W_3 are set to 1.0, 1.0, and 10^5 for each loss term, respectively. This allows for each loss to be on the same scale.

The prediction performance of the trained ANN is preliminarily assessed using a different random dataset, generated by replicating all the above procedures. A commendable agreement between the predicted and target values is illustrated in Fig. 4, where root mean square error (RMSE) is included. Meanwhile, a comparable agreement in laminar flame speed under different equivalence ratios is observed (not shown here) between the trained ANN and the direct integration of

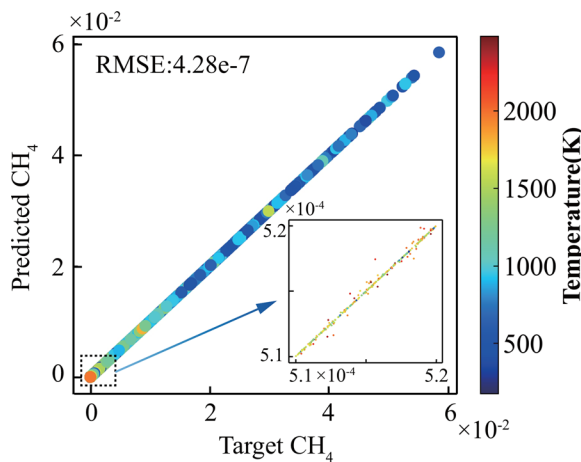


FIG. 4. MLP predictions for CH_4 colored by the temperature of the sample.

ODE. All these establish the applicability of the trained ANN for subsequent assessments in the swirling flames. To demonstrate that the trained ANN is not case-specific, simulations of the XJTU swirl flame and the Cambridge swirling stratified premixed flame will be presented.

III. APPLICATION TO XJTU SWIRLING FLAME

A. Configuration of XJTU swirl combustor and numerical methods

Figure 5 shows the configuration of the XJTU swirl combustor. The combustor is composed of three main parts: a premixing chamber, a 12-vane swirl set at a 45° angle, and a quartz liner. Methane (CH_4) and air undergo thorough mixing within the premixing chamber. The swirler with 12 vanes and 45° vane angle is used to create a swirling flow to stabilize the flame. The quartz liner with the dimensions of $70 \times 70 \times 180 \text{ mm}^3$ is used to provide both flame visibility and access

for laser diagnostic. In this study, a stoichiometrically premixed methane-air mixture, with an average velocity of 5 m/s , is channeled through the swirler. This process produces a highly swirling flow with a swirl number of 0.71 . The detailed structure of this combustor can be found in Refs. 50 and 51.

The computational domain corresponds to the experimental setup, as illustrated in Fig. 5. A nonuniform grid with a total of 5.0×10^6 cells is employed. The mesh refinement is specifically applied to the flame region with cell size less than 0.4 mm . The mesh resolution employed here has been verified by referenced studies^{39,51,52} to be adequate for achieving a high resolution in the flame region. In the current study, the gas-phase flow field is resolved by employing Favre-filtered compressible Navier-Stokes equations, which are coupled with a Smagorinsky model for sub-grid-scale stress. The coefficients $C_e = 1.048$ and $C_k = 0.094$ of the Smagorinsky model are retained as the default values in OpenFOAM. The interaction between turbulence and combustion chemistry is modeled using the partially stirred reactor (PaSR) combustion model. The reacting fraction in the PaSR model is determined by a function of both mixing timescale (t_{mix}) and chemical timescale (t_c) and can be expressed as

$$\gamma = \frac{t_c}{t_c + t_{mix}}. \quad (12)$$

In this equation, t_c is determined by the slowest species formation rate.⁵³ This estimation can be expressed as

$$t_c = \max \left(\frac{Y_k}{\dot{\omega}_k} \right), \quad (13)$$

where Y_k and $\dot{\omega}_k$ are the mass fraction and formation rate of k_{th} species, respectively. On the other hand, t_{mix} is derived from the geometric mean of the Taylor and Kolmogorov scales.⁵⁴ The corresponding expression is written as

$$t_{mix} = \sqrt{\frac{\bar{k}_{sgs}}{\varepsilon} \left(\frac{\nu}{\varepsilon} \right)^{\frac{1}{2}}}, \quad (14)$$

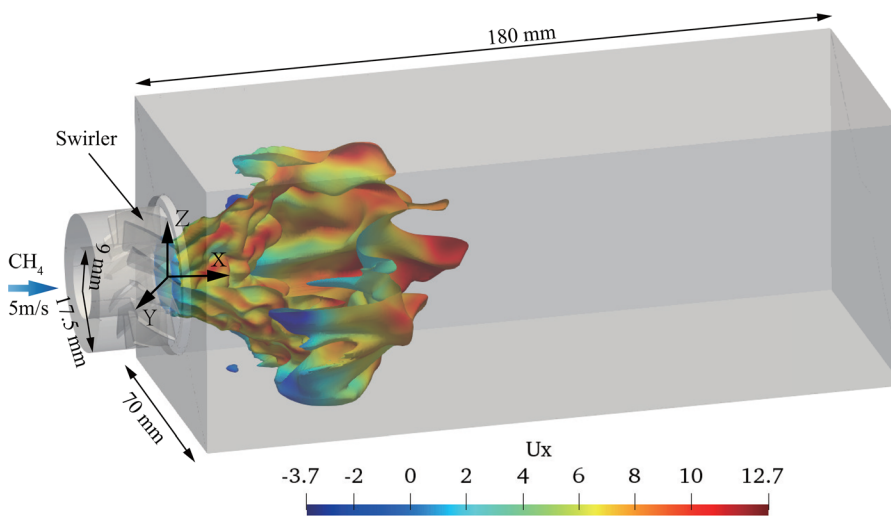


FIG. 5. Computational domain of XJTU burner. The iso-surface of flame temperature of 2000 K colored by axial velocity.

where k_{sgs} , ν , and ε denote the sub-grid kinetic energy, kinematic viscosity, and dissipation rate of kinetic energy, respectively.

It is important to note that the ANN model only substitutes the direct integration of source terms within the PaSR model, rather than replacing the PaSR model entirely. The momentum and scalars are discretized in space with second-order schemes. All walls utilize no-slip boundary conditions to replicate physical realism. At the fuel inlet, we introduce pseudo-turbulent fluctuations via a sophisticated random spot method for turbulence generation.⁵⁵ The integral length scale and fluctuation intensity are consistent with those documented in referenced works.⁵⁶

B. Results and discussion for XJTU swirling premixed flame

In this study, simulations are carried out using two distinct methodologies: the CPU-DI and GPU-ANN. The CPU-DI method utilizes a CPU-based solver for the resolution of flow and scalar equations, integrating reaction sources through the CVODE solver. Conversely, the GPU-ANN method employs a GPU-based solver, with a trained ANN predicting reaction rates. Note that the CPU/GPU-based solvers share identical governing equations and numerical modeling.

In this section, the macro flame structure, such as flame height, combustion intensity, and the distribution of radical species, is first compared to evaluate the predictive performance of the GPU-ANN approach. The height of the flame is a critical attribute in characterizing the overall structure of a flame. In line with the definition of Singh *et al.*,⁵⁷ the height of the flame corresponds to the edge of the reaction zone, as clearly evidenced by the hydroxyl radical (OH) distribution. Figure 6(a) illustrates the comparison of time-averaged OH distribution between the experimental measurements and the predictions from the GPU-ANN and CPU-DI approaches. Due to the absence of laser sheet nonuniformity correction, the experimental results fail to accurately depict the relative concentration of OH radicals. It should be noted that the fluorescence intensity of OH is scaled to [0, 0.005] for OH-PLIF (planar laser-induced fluorescence), while for simulation results, it represents OH mass fraction. It is evident that both

approaches predict similar flame height as the experimental measurement. In addition, both simulation results capture the sharp increase in OH intensity near the flame surface region, indicating that the GPU-ANN approach is capable of identifying the reaction location in a premixed flame. Considering that the OH intensity does not necessarily imply the combustion intensity and the experimental results fail to accurately depict the relative concentration of OH radicals due to the absence of laser sheet nonuniformity correction, the flame surface density (Σ) obtained from the experiments, as well as the GPU-ANN and CPU-DI approaches are thus compared in Fig. 6(b). In the experiment, the Σ is determined through a statistical approach by analyzing 300 instantaneous OH-PLIF images. Flamelets are extracted from these images and superimposed to form a flame brush, which is then used to calculate the two-dimensional Σ . The detailed procedures can be found in the study by Mao *et al.*⁵⁸ As for the simulations, the generalized Σ is calculated as $\Sigma = |\nabla c|$, $c = Y_{CO_2} + Y_{CO}$. A similar distribution of the Σ shown in Fig. 6(b) indicates the combustion intensities are reasonably captured using the CPU-DI and GPU-ANN approaches.

A further evaluation of the GPU-ANN approach is to compare the macro flame structure in terms of the distribution of temperature and key radical species. The three-dimensional (3D) topology of premixed flame is presented in Fig. 7 where the iso-surface of different progress variables (PV) is colored by the flame temperature. The topology structures of the flame under different PVs appear similar between the CPU-DI and GPU-ANN approaches. Additionally, the range of flame temperature at each PV state remains the same for both approaches. This indicates that the GPU-ANN approach is capable of reproducing the evolution of the flame with respect to the PV. Figure 8 shows the distributions of formaldehyde $CH_2O-OH-CH_4$ at axial locations of 0 and 30 mm for the CPU-DI and GPU-ANN cases. At $X = 0$ mm, in both the CPU-DI and GPU-ANN scenarios, the findings reveal a uniform distribution of the wrinkled flame along the circumferential direction, marked by twelve convex regions that align with the number of vanes. These regions exhibit a lower equivalence ratio, pointing to accelerated fuel consumption attributable to stretch effects.⁵⁹ As the axial distance increases to 30 mm, it is apparent that CH_2O is encompassed by OH, while CH_4 is encompassed by CH_2O .

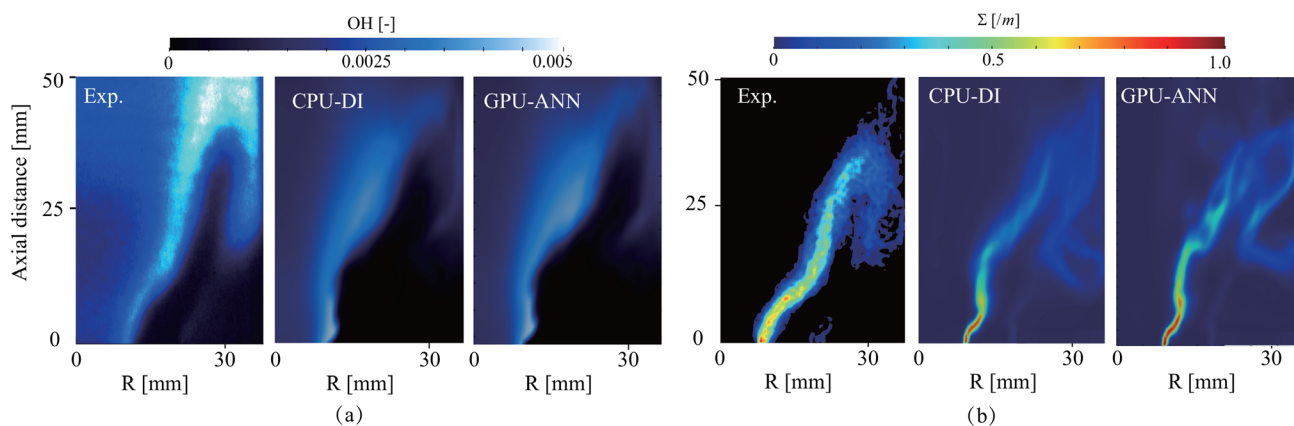


FIG. 6. Comparison of (a) time-averaged OH-PLIF and simulated OH mass fraction using the CPU-DI and GPU-ANN approaches as well as (b) measured and simulated flame surface intensities (Σ) using the CPU-DI and GPU-ANN approaches.

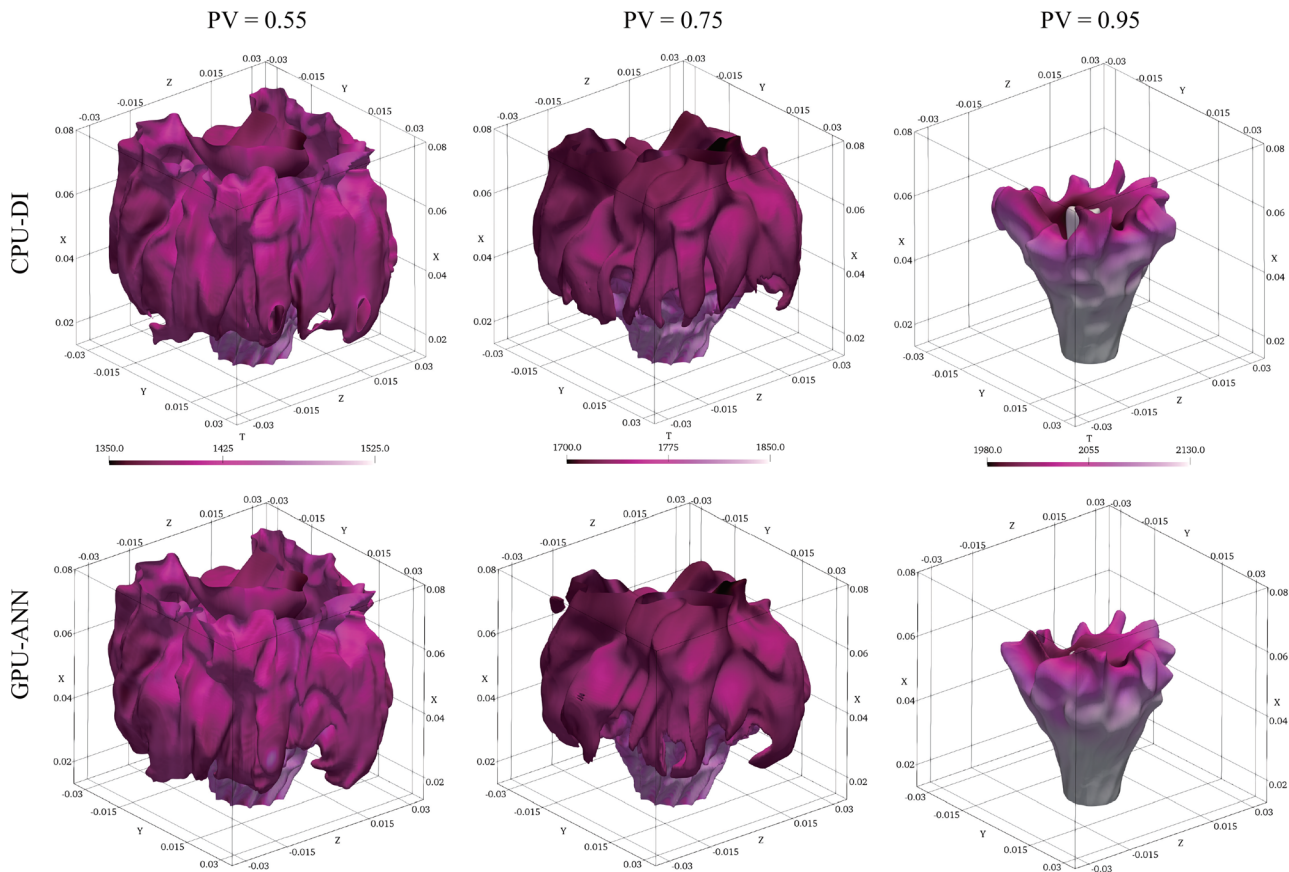


FIG. 7. Comparison of iso-surface of progress variables of 0.55, 0.75, and 0.95 at 12 ms between the CPU-DI and GPU-ANN approaches.

15 July 2024 11:46:55

The highest OH concentration is predominantly located at the equivalence ratio of 0.85. Within the center of the flame, a lower equivalence ratio is observed, which is likely a result of entrainment bringing the downstream mixture into the recirculation zone. All these observations are consistent across both the CPU-DI and GPU-ANN scenarios. This consistency provides solid evidence that the GPU-ANN approach is capable of predicting the macro flame structures as effectively as the traditional CPU-DI approach.

IV. APPLICATION TO CAMBRIDGE HIGH-SWIRLING STRATIFIED FLAME

The proposed GPU-AI approach is qualitatively evaluated in premixed swirling flame by comparing the macro flame structure in Sec. III. In this section, this approach will be applied to Cambridge swirling stratified premixed flame, designed by Sweeney *et al.*,^{40,60} to further assess its performance with robust statistical analysis of scalars. Initially, both mean and root mean square (RMS) data are time-averaged over a duration approximately equivalent to three complete flow-through times, based on the inner jet velocity and an axial extent of 40 mm. An additional averaging is performed in the azimuthal direction. Furthermore, the analysis of scatters in temperature-species space is performed.

A. Configuration of Cambridge swirling stratified premixed flame and numerical methods

Compared to the study by Readshaw *et al.*,²⁹ a higher swirl ratio case SWB7 is simulated here. Figure 9 shows the scheme view of the Cambridge burner. The burner incorporates a central bluff body accompanied by dual annular fuel jets. Airflow is facilitated at the burner's exterior. The external fuel jet can provide varied swirling flows, characterized by swirl numbers, which denote the ratio of averaged tangential velocity to averaged axial velocity. The major parameters of the case SWB7 are presented in Table II. The scalars were measured using multi-scalar laser diagnostics in Sandia National Laboratories. Specifically, temperatures were measured via Rayleigh scattering, and major species were measured using Raman scattering and laser-induced fluorescence (CO-LIF) at 103 μm projected pixel resolution. More detailed experimental setup and measurement methods are available in Ref. 60.

The computational domain is a cylindrical domain with the dimensions of 300 mm \times 100 mm \times 2π in axial, radial, and azimuthal directions, respectively. The 2.5×10^6 mesh cells are employed. As shown in Fig. 9, a refined mesh with cell size less than 0.25 mm is applied to cover the flame region, which can provide enough resolution based on the mesh size used in Refs. 61 and 62. The numerical

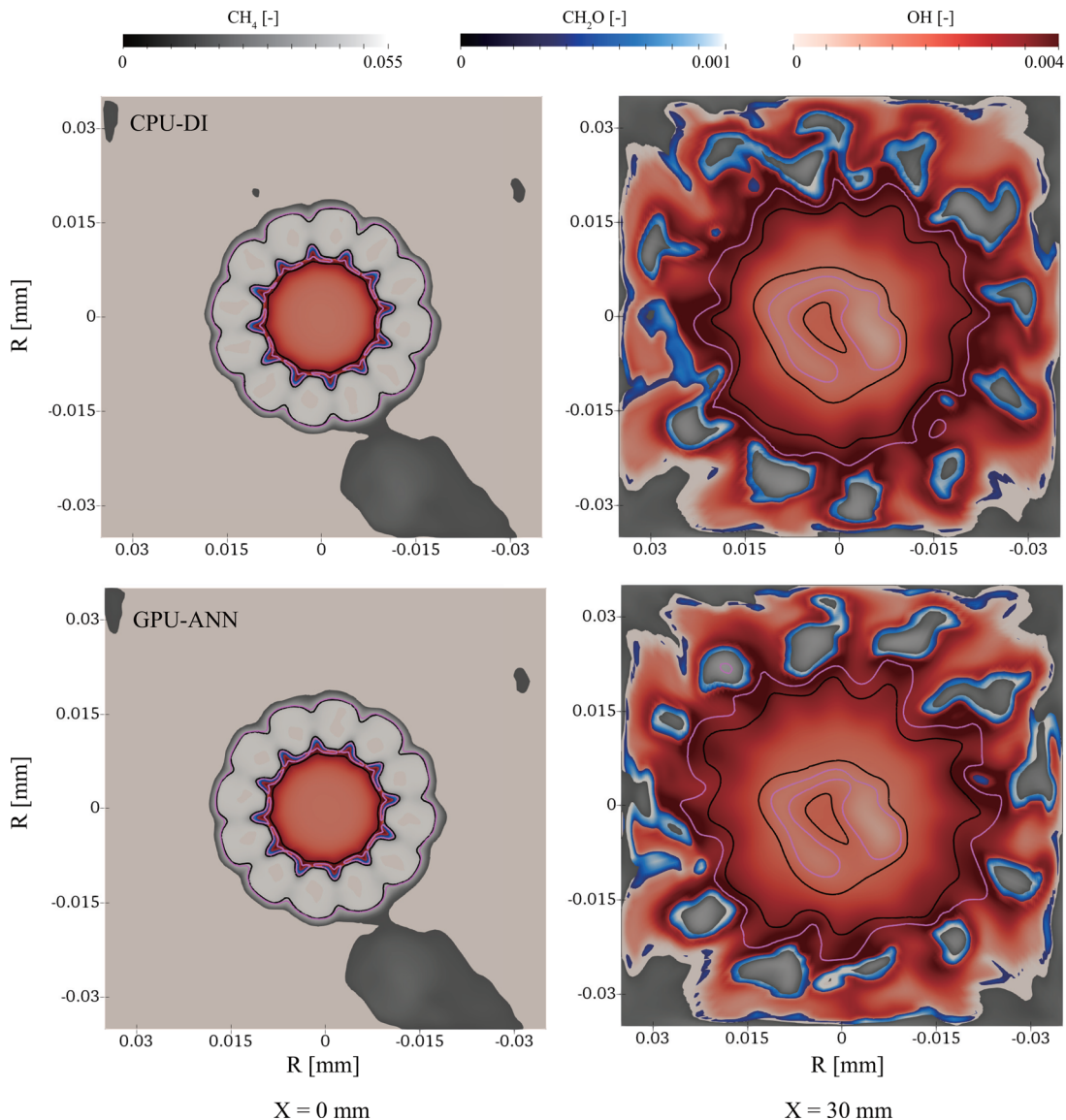


FIG. 8. Comparison of the distributions of $\text{CH}_4\text{-OH-CH}_2\text{O}$ at 12 ms for different axial locations of 0 and 30 mm in the CPU-DI and GPU-ANN cases. The magenta and black lines represent the equivalence ratio of 0.85 and 0.90, respectively. The range of iso-surface of CH_4 , CH_2O , and OH are $[0.02, 0.055]$, $[0.4 \times 10^{-3}, 1.2 \times 10^{-3}]$, and $[0, 4 \times 10^{-3}]$, respectively.

methods and turbulence inlet boundary conditions employed in this case are the same as those used in Sec. III.

B. Results and discussion for Cambridge swirling stratified premixed flame

While Sec. III has already shown that the macro flame structure can be accurately captured with the GPU-ANN approach in the swirling flame, it is unclear whether the statistical characteristics can be accurately captured in the more complicated swirling stratified flame case (SWB7). This will be explored in the subsequent discussion.

The mean and RMS statistics for the SWB7 case are presented in Figs. 10 and 11. The mean and RMS values are identified using the black and red colors, respectively. Solid lines illustrate outcomes from the CPU-DI approach, and dashed lines correspond to the GPU-ANN approach. The circles are used to denote the experimental mean and RMS data.⁶⁰ Figure 10 shows the simulated scalar profiles of the temperature, mass fraction of CH_4 , carbon dioxide (CO_2), oxygen (O_2), carbon monoxide (CO), and water (H_2O) and compares them to the corresponding experimental data at four different axial locations. It is clear that the simulated results from the GPU-ANN approach are almost identical to those from the CPU-DI approach. This suggests

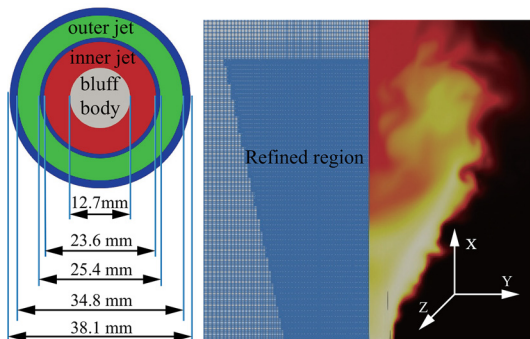


FIG. 9. Dimension of the Cambridge burner and mesh configuration used in the simulation.

TABLE II. Main parameters for Cambridge burner SWB7.

U_o (m/s)	U_i (m/s)	U_{co} (m/s)	ϕ_i	ϕ_o	Swirl (%)
8.3	18.7	0.4	1.0	0.5	0.79

that the GPU-ANN method is capable of replicating the key combustion characteristics modeled by the traditional CPU-DI approach, even under the complicated swirling flow conditions. As compared to the experimental results, good agreements between the experimental and simulated results are observed from axial location 10 to 30 mm. However, there some discrepancies are shown for 40 mm. Specifically, the peak value of the temperature is under-predicted by 200 K. This consequently leads to a lower prediction of H_2O and CO_2 . The possible reason could be attributed to an overestimation of the recirculation flow intensity, leading to enhanced mixing with the air downstream.⁶³ This is evident from the observed profiles of O_2 , where a higher concentration of O_2 is predicted within the recirculation zone. To quantify the simulation errors compared to the experimental data, quantitative indicators are presented here. The maximum relative error for the mean statistics from axial location 10 to 30 mm is less than 10% except for the temperature and CO at axial location 10 mm, while this value almost reaches 30% at axial location 40 mm. As far as the RMS statistics are concerned, the maximum relative error of 40% is observed at axial location 20 mm. Nevertheless, the relative errors are still within the reasonable range as compared to the simulation results in Refs. 62 and 64. It is important to mention that the primary goal of this work is not to directly compare simulation outcomes with the experimental data. A further investigation of the effects of swirl on the flow and flame structure of the recirculation zone falls beyond the scope of this study.

The minor species in the chemical reaction system cover a wider range of orders of magnitude in the thermochemical phase space, presenting a more significant challenge to the ANN's predictive capabilities than the major species. Consequently, it is crucial to conduct a more thorough assessment of the GPU-ANN approach's accuracy in predicting these minor species. Figure 11 shows the radial mean and

RMS profiles of several minor species with mass fractions spanning from the order of 10^{-3} to 10^{-5} . Overall, the mass fraction of all species simulated by the GPU-ANN approach shows a good agreement with the simulation results obtained from the CPU-DI approach. However, it is clear that the predictive performance of the GPU-ANN approach for minor species does not match the strength demonstrated for major species, as illustrated in Fig. 10. Specifically, there are slight discrepancies in the descending order of the mass fractions. For instance, the mass fraction of methylene (CH_2) with the order of 10^{-5} is underpredicted by approximately 10% at the axial location of 10 and 20 mm. In the study by Readshaw *et al.*,²⁹ the predicted outcomes for minor species, whose mass fractions are on the order of 10^{-5} obtained using the ANN method, closely align with those derived from the DI method. This congruence is likely attributable to the RMSE of the ANN (10^{-8}) obtained in their study, compared to the order of 10^{-7} noted in the current study. However, if there is no particular interest in these relatively small mass fractions of the species involved, the prediction error observed with the GPU-ANN approach is considered acceptable.

Beyond the statistical characteristics of the scalar, scatter distribution in temperature-species at a single instant is also a crucial metric for evaluating the performance of the GPU-ANN approach. Figure 12 compares the scatter plots for the mass fraction of CH_4 , CO , CO_2 , H_2 , H_2O , and O_2 in the temperature space at axial location of 10 and 30 mm between the GPU-ANN and CPU-DI approaches. All scatters are colored by the equivalence ratio ranging from 0.65 to 1.0. At the axial location of 10 mm, most of the scatter points are concentrated around the stoichiometric state, with only a few scatters around the equivalence ratio of 0.8 for both the GPU-ANN and CPU-DI approaches. As the downstream distance increases to 30 mm, discrepancies between CPU-DI and GPU-ANN are observed for intermediate products (CO and H_2) at the axial location of 30 mm, particularly noticeable with more scattered points when the equivalence ratio is close to 1.0 in GPU-ANN's predictions. The possible reason can be attributed to the turbulence fluctuation in the LES simulation, since the scatter distributions of CO and H_2 are similar at some other time instances (not shown here). It should be noted that numerous scatter points with low equivalence ratios are predicted by both the GPU-ANN and CPU-DI approaches, particularly at temperatures greater than 1500 K. This pattern, arising from entrainment, highlights the GPU-ANN approach's adeptness in capturing the local structure of the swirling flame.

V. COMPUTATIONAL SAVING

It is expected that the GPU-ANN approach is able to significantly decrease the computational cost. This is illustrated in Figs. 13 and 14, where the total, flow, and chemistry time expenses of a single time step are compared between the CPU-DI and GPU-ANN approaches for the XJTU and SWB7 swirling flame cases. The cases involving the GPU-ANN are executed using a single GPU card, whereas the cases employing the CPU-DI method are conducted on a node with 32 CPU cores. It should be noted that training the ANN for 1600 epochs on a single GPU card took less than 2 h, which is negligible compared to the overall computational costs. The training cost is hence not included in Figs. 13 and 14. Since the ANN is employed solely to replace the integration of ODEs, the computational savings in chemistry calculations are primarily attributed to the ANN, whereas savings in flow computations are mainly due to the GPU. As shown in

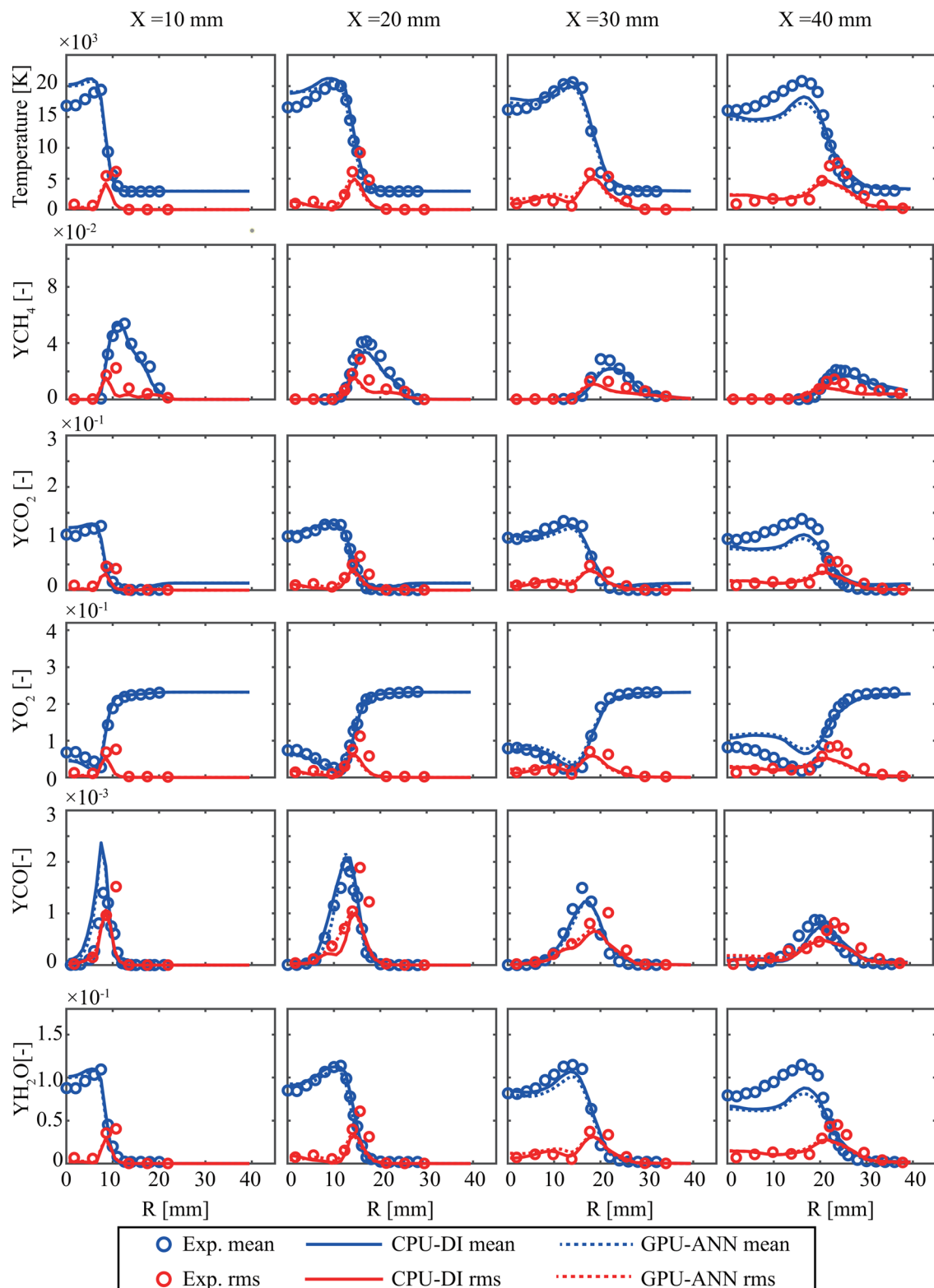


FIG. 10. Radial profiles of mean and RMS for temperature and major species mass fraction at four different axial locations in the experiment, CPU-DI, and GPU-ANN cases.

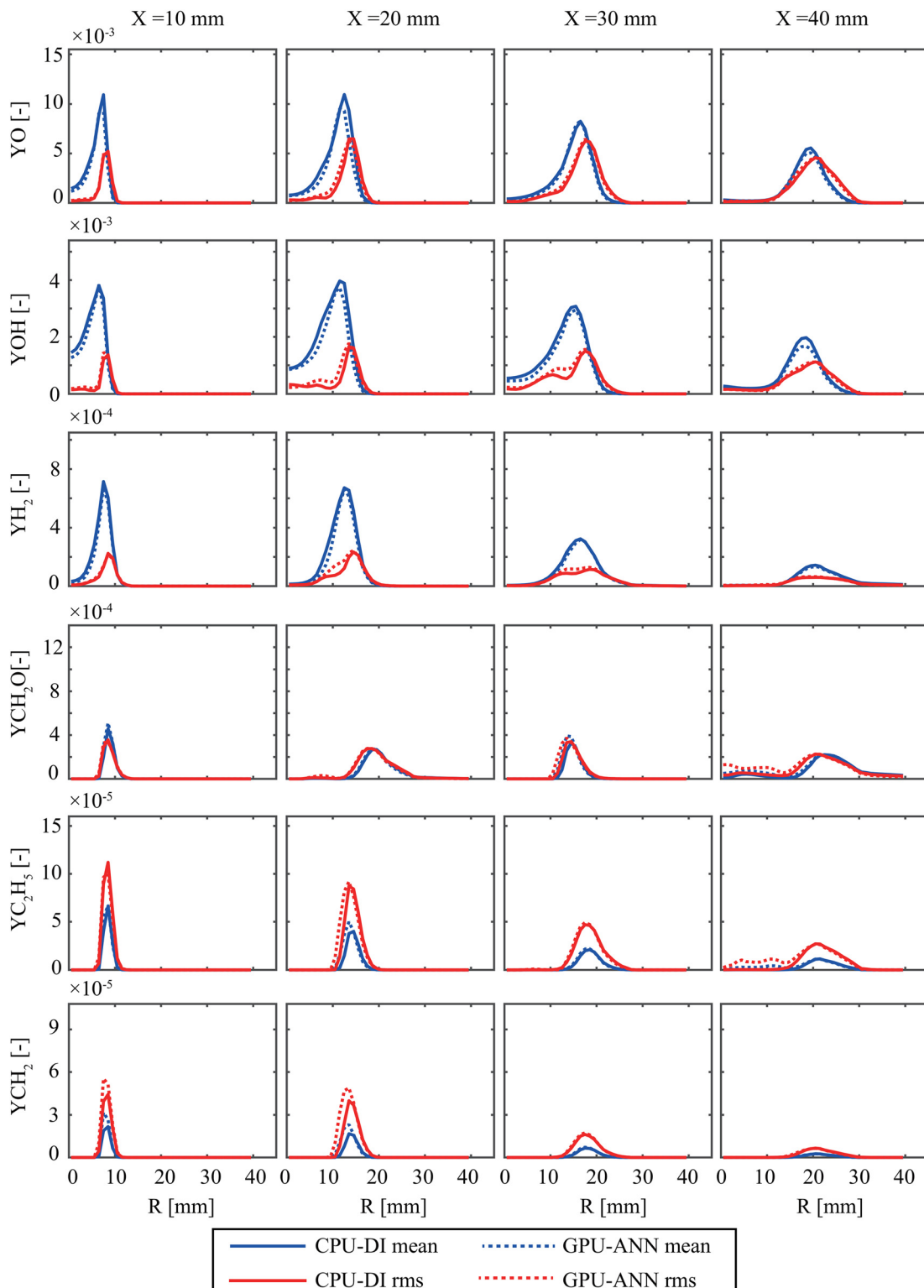


FIG. 11. Radial profiles of mean and RMS for minor species mass fraction across the order from 10^{-3} to 10^{-5} at four different axial locations in the experiment, CPU-DI, and GPU-ANN cases.

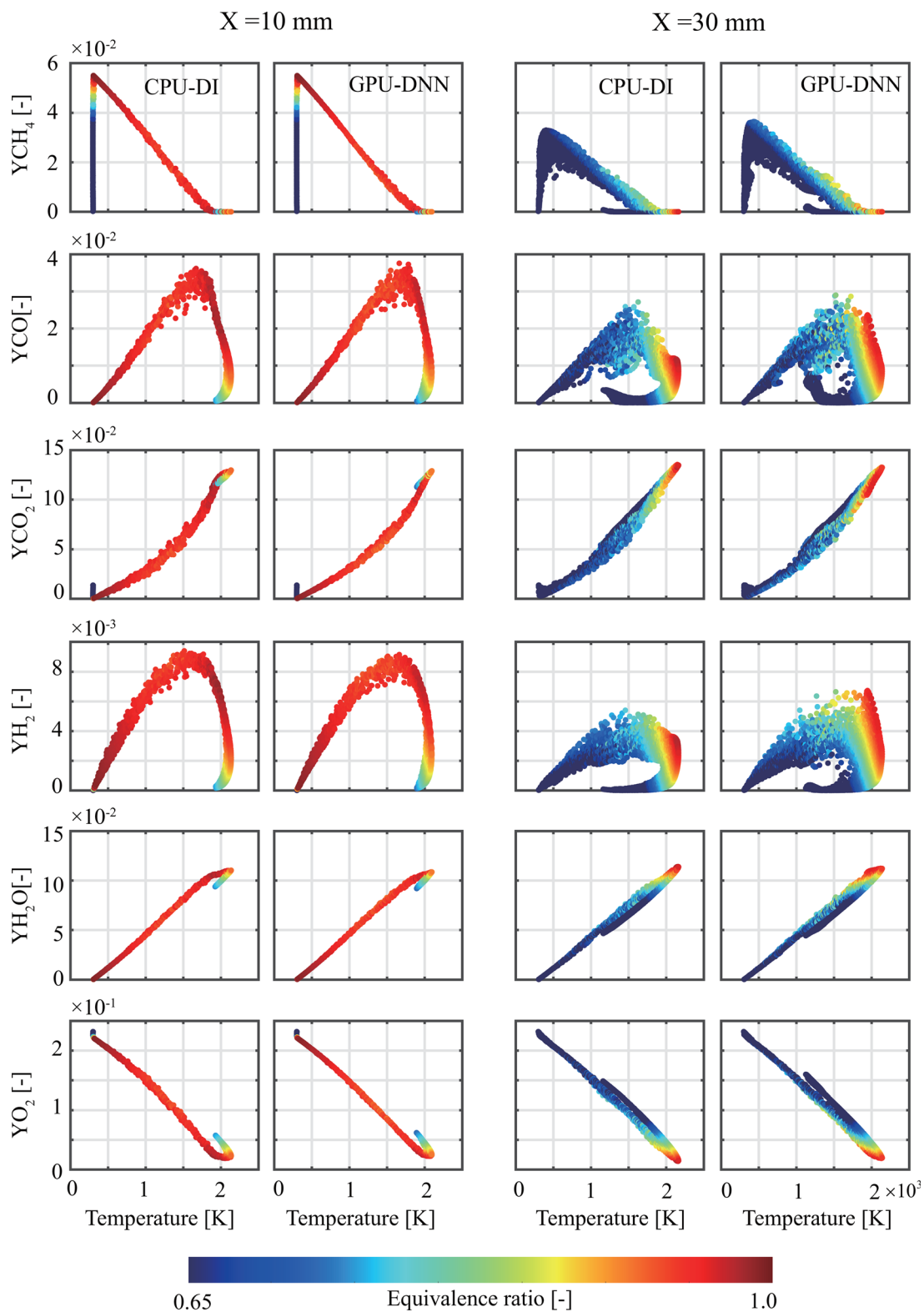


FIG. 12. Instantaneous scatter plots of key species mass fraction over flame temperature for CPU-DI and GPU-ANN at axial locations $X = 10, 30 \text{ mm}$.

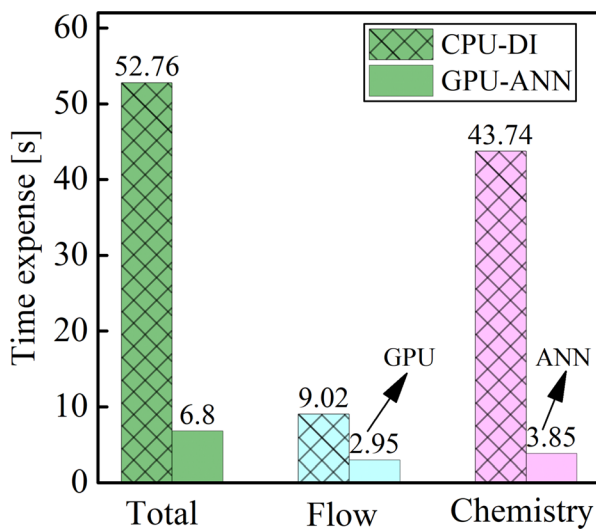


FIG. 13. Time expense for CPU-DI (32 cores) and GPU-ANN (1 card) approaches in the XJTU swirling flame case.

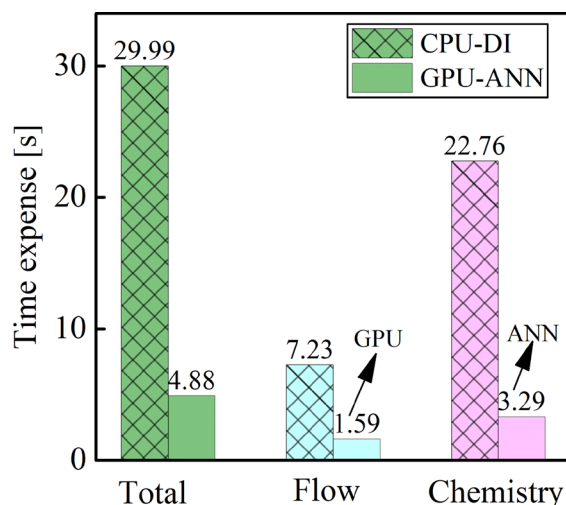


FIG. 14. Time expense for CPU-DI (32 cores) and GPU-ANN (1 card) approaches in the Cambridge swirling stratified flame case.

Figs. 13 and 14, the use of GPU-ANN significantly enhances computational efficiency for both the XJTU and Cambridge swirling flames. With the GPU-ANN, the XJTU swirling flame sees a time reduction of 91.2% for chemical reactions and 67.3% for flow computations, giving a 1GPU-to-1CPU speed-up ratio of 363 and 98 compared to the CPU-DI method. Meanwhile, the Cambridge swirling stratified flame benefits from 85.5% and 78.0% time savings in chemistry and flow calculations, respectively, with speed-ups of 221:1 and 145:1 under the same comparison. In these two cases of swirling flames, the computation of a single step with one GPU-ANN card is approximately seven times quicker than using a CPU-DI with 32 cores. Although there is a marked reduction in time spent on chemistry sources, it still accounts for 60% of the

total time in both swirling flame cases. This proportion may rise with the scaling of inference points. Consequently, optimizing the inference framework and minimizing the ANN's parameters is essential to achieve further speedup in future work.

VI. CONCLUSION

In the present study, two LES of swirling flames including the XJTU swirling flame and the Cambridge swirling stratified flame are conducted to evaluate the proposed GPU-ANN approach. This method involves the ANN model that is trained using 1D laminar flame solutions augmented with random perturbations and then implemented within the solver that is fully accelerated by GPU and based on OpenFOAM.

The results of the simulations reveal a strong alignment between the GPU-ANN method and the traditional approach using the CPU solver with direct integration of chemistry, in terms of capturing the macro flame structure and statistical characteristics such as average and RMS of scalar fields and scattered instantaneous points. This consistency suggests that the GPU-ANN method can achieve a level of accuracy comparable to that of the standard CPU-DI solver even in complex scenarios. Furthermore, the computational savings achieved by the GPU-ANN approach have been evaluated. The results demonstrate that for the Cambridge swirling flame, time spent on chemistry and flow calculations is reduced by 85.5% and 78.0%, respectively, when using one GPU card as opposed to 32 CPU cores. For the XJTU swirling flame, the corresponding time reductions of 91.2% for chemistry and 67.3% for flow computations were observed under the same comparison. This corresponds to a speed-up factor exceeding two orders of magnitude.

The present study showcases the potential for widespread application of the proposed GPU-ANN approach in combustion simulations that tackle various complex scenarios using detailed chemistry, while also substantially cutting computational costs. However, it should be noted that the time spent on chemistry sources still accounts for 60% of the total time. Future work will be focused on optimizing the inference framework and minimizing the ANN's parameters.

ACKNOWLEDGMENTS

This work is supported by the National Natural Science Foundation of China (Grant Nos. 92270203, 52276096, and 523B2062), GHfund C (No. 202302032372), CCF-Baidu Open Fund (No. 202301), the “Emerging Engineering Interdisciplinary-Young Scholars Project, Peking University,” and the China Postdoctoral Science Foundation (No. 2023Mu40056). The support from the Royal Society (No. IEC/NSFC/223421) is also acknowledged. This work used the Performance Computing Platform of CAPT of Peking University.

AUTHOR DECLARATIONS

Conflict of Interest

The authors have no conflicts to disclose.

Author Contributions

Min Zhang: Conceptualization (lead); Software (equal); Validation (lead); Writing – original draft (lead). **Runze Mao:** Conceptualization (equal); Software (equal). **Han Li:** Methodology (equal); Writing –

review & editing (supporting). **Zhenhua An:** Resources (equal); Software (equal). **Zhi X. Chen:** Funding acquisition (lead); Software (equal); Supervision (lead); Writing – review & editing (lead).

DATA AVAILABILITY

The data that support the findings of this study are available from the corresponding authors upon reasonable request.

REFERENCES

- ¹T. Poinot, "Prediction and control of combustion instabilities in real engines," *Proc. Combust. Inst.* **36**, 1–28 (2017).
- ²M. E. Mueller and H. Pitsch, "Large eddy simulation of soot evolution in an aircraft combustor," *Phys. Fluids* **25**, 110812 (2013).
- ³V. Raman and M. Hassanaly, "Emerging trends in numerical simulations of combustion systems," *Proc. Combust. Inst.* **37**, 2073–2089 (2019).
- ⁴A. Avdić, G. Kuenne, F. di Mare, and J. Janicka, "LES combustion modeling using the Eulerian stochastic field method coupled with tabulated chemistry," *Combust. Flame* **175**, 201–219 (2017).
- ⁵N. Peters, *Turbulent Combustion*, Cambridge Monographs on Mechanics (Cambridge University Press, 2001).
- ⁶J. Chen, W. Kollmann, and R. Dibble, "PDF modeling of turbulent nonpremixed methane jet flames," *Combust. Sci. Technol.* **64**, 315–346 (1989).
- ⁷J. Van Oijen and L. D. Goey, "Modelling of premixed laminar flames using flamelet-generated manifolds," *Combust. Sci. Technol.* **161**, 113–137 (2000).
- ⁸H. Bao, N. Maes, H. Y. Akargun, and B. Somers, "Large eddy simulation of cavitation effects on reacting spray flames using FGM and a new dispersion model with multiple realizations," *Combust. Flame* **236**, 111764 (2022).
- ⁹M. E. Mueller, "Physically-derived reduced-order manifold-based modeling for multi-modal turbulent combustion," *Combust. Flame* **214**, 287–305 (2020).
- ¹⁰A. S. Newale, P. Sharma, S. B. Pope, and P. Pepiot, "A feasibility study on the use of low-dimensional simulations for database generation in adaptive chemistry approaches," *Combust. Theor. Model.* **26**, 1239–1261 (2022).
- ¹¹U. Maas and S. B. Pope, "Implementation of simplified chemical kinetics based on intrinsic low-dimensional manifolds," *Symp. (Int.) Combust.* **24**, 103–112 (1992).
- ¹²S. B. Pope, "Computationally efficient implementation of combustion chemistry using in situ adaptive tabulation," *Combust. Theory Model.* **1**, 41–63 (1997).
- ¹³A. Ketelheun, C. Olbricht, F. Hahn, and J. Janicka, "NO prediction in turbulent flames using LES/FGM with additional transport equations," *Proc. Combust. Inst.* **33**, 2975–2982 (2011).
- ¹⁴L. Zhou, Y. Song, W. Ji, and H. Wei, "Machine learning for combustion," *Energy AI* **7**, 100128 (2022).
- ¹⁵M. Ihme, W. T. Chung, and A. A. Mishra, "Combustion machine learning: Principles, progress and prospects," *Prog. Energy Combust. Sci.* **91**, 101010 (2022).
- ¹⁶F. Christo, A. Masri, E. Nebot, and T. Turányi, "Utilising artificial neural network and repro-modelling in turbulent combustion," in *Proceedings of ICNN'95—International Conference on Neural Networks* (IEEE, 1995), Vol. 2, pp. 911–916.
- ¹⁷T. S. Brown, H. Antil, R. Löhner, F. Togashi, and D. Verma, "Novel DNNs for stiff ODEs with applications to chemically reacting flows," in *International Workshops on High Performance Computing* (Springer, 2021), pp. 23–39.
- ¹⁸E. L. Petersen and R. K. Hanson, "Reduced kinetics mechanisms for ram accelerator combustion," *J. Propul. Power* **15**, 591–600 (1999).
- ¹⁹J. A. Blasco, N. Fueyo, C. Dopazo, and J. Chen, "A self-organizing-map approach to chemistry representation in combustion applications," *Combust. Theory Model.* **4**, 61 (2000).
- ²⁰J. Blasco, N. Fueyo, C. Dopazo, and J. Ballester, "Modelling the temporal evolution of a reduced combustion chemical system with an artificial neural network," *Combust. Flame* **113**, 38–52 (1998).
- ²¹A. Parente, J. C. Sutherland, L. Tognotti, and P. J. Smith, "Identification of low-dimensional manifolds in turbulent flames," *Proc. Combust. Inst.* **32**, 1579–1586 (2009).
- ²²S. Abdelwahid, M. R. Malik, H. A. A. K. Hammoud, F. E. Hernández-Pérez, B. Ghanem, and H. G. Im, "Large eddy simulations of ammonia-hydrogen jet flames at elevated pressure using principal component analysis and deep neural networks," *Combust. Flame* **253**, 112781 (2023).
- ²³L. Castellanos, R. S. M. Freitas, A. Parente, and F. Contino, "Deep learning dynamical latencies for the analysis and reduction of combustion chemistry kinetics," *Phys. Fluids* **35**, 107143 (2023).
- ²⁴S. Goswami, A. D. Jagtap, H. Babaee, B. T. Susi, and G. E. Karniadakis, "Learning stiff chemical kinetics using extended deep neural operators," *Comput. Methods Appl. Mech. Eng.* **419**, 116674 (2024).
- ²⁵J. An, G. He, K. Luo, F. Qin, and B. Liu, "Artificial neural network based chemical mechanisms for computationally efficient modeling of hydrogen/carbon monoxide/kerosene combustion," *Int. J. Hydrogen Energy* **45**, 29594–29605 (2020).
- ²⁶Y. Weng, Z. Zhao, H. Zhang, and D. Zhou, "Extending Fourier neural operators to learn stiff chemical kinetics," *40th International Symposium on Combustion* (submitted) (2024).
- ²⁷T. Zhang, Y. Yi, Y. Xu, Z. X. Chen, Y. Zhang, E. Weinan, and Z.-Q. J. Xu, "A multi-scale sampling method for accurate and robust deep neural network to predict combustion chemical kinetics," *Combust. Flame* **245**, 112319 (2022).
- ²⁸Z.-Q. J. Xu, J. Yao, Y. Yi, L. Hang, Y. Zhang, T. Zhang *et al.*, "Solving multiscale dynamical systems by deep learning," *arXiv:2401.01220* (2024).
- ²⁹T. Readshaw, L. L. Franke, W. Jones, and S. Rigopoulos, "Simulation of turbulent premixed flames with machine learning-tabulated thermochemistry," *Combust. Flame* **258**, 113058 (2023).
- ³⁰T. Ding, T. Readshaw, S. Rigopoulos, and W. Jones, "Simulation of turbulent premixed flames with machine learning-tabulated thermochemistry," *Combust. Flame* **231**, 111493 (2021).
- ³¹T. Ding, S. Rigopoulos, and W. Jones, "Machine learning tabulation of thermochemistry of fuel blends," *Appl. Energy Combust. Sci.* **12**, 100086 (2022).
- ³²A. Liu, T. Ding, R. Liu, S. Rigopoulos, and K. Luo, "Machine learning tabulation of thermochemistry for turbulent dimethyl ether (DME) flames," *Fuel* **360**, 130338 (2024).
- ³³F. E. H. Pérez, N. Mukhadiyev, X. Xu, A. Sow, B. J. Lee, R. Sankaran, and H. G. Im, "Direct numerical simulations of reacting flows with detailed chemistry using many-core/GPU acceleration," *Comput. Fluids* **173**, 73–79 (2018).
- ³⁴R. Bielawski, S. Barwey, S. Prakash, and V. Raman, "Highly-scalable GPU-accelerated compressible reacting flow solver for modeling high-speed flows," *Comput. Fluids* **265**, 105972 (2023).
- ³⁵L. Esclapez, M. Day, J. Bell, A. Felden, C. Gilet, R. Grout, M. H. de Frahan, E. Motheau, A. Nonaka, L. Owen *et al.*, "PeleLMEx: An AMR low Mach number reactive flow simulation code without level sub-cycling," *J. Open Source Softw.* **8**, 5450 (2023).
- ³⁶M. T. Henry de Frahan, J. S. Rood, M. S. Day, H. Sitaraman, S. Yellapantula, B. A. Perry, R. W. Grout, A. Almgren, W. Zhang, J. B. Bell *et al.*, "PeleC: An adaptive mesh refinement solver for compressible reacting flows," *Int. J. High Perform. Comput. Appl.* **37**, 115–131 (2023).
- ³⁷H. P. Le, J.-L. Cambier, and L. K. Cole, "GPU-based flow simulation with detailed chemical kinetics," *Comput. Phys. Commun.* **184**, 596–606 (2013).
- ³⁸J. M. Levesque, R. Sankaran, and R. Grout, "Hybridizing S3D into an exascale application using OpenACC: An approach for moving to multi-petaflops and beyond," in *SC'12: Proceedings of the International Conference on High Performance Computing, Networking, Storage and Analysis* (IEEE Computer Society Press, 2012), pp. 1–11.
- ³⁹Z. An, M. Zhang, W. Zhang, R. Mao, X. Wei, J. Wang, Z. Huang, and H. Tan, "Emission prediction and analysis on CH₄/NH₃/air swirl flames with LES-FGM method," *Fuel* **304**, 121370 (2021).
- ⁴⁰M. S. Sweeney, S. Hochgreb, M. J. Dunn, and R. S. Barlow, "The structure of turbulent stratified and premixed methane/air flames. II: Swirling flows," *Combust. Flame* **159**, 2912–2929 (2012).
- ⁴¹R. Mao, M. Lin, Y. Zhang, T. Zhang, Z.-Q. J. Xu, and Z. X. Chen, "DeepFlame: A deep learning empowered open-source platform for reacting flow simulations," *Comput. Phys. Commun.* **291**, 108842 (2023).
- ⁴²H. G. Weller, G. Tabor, H. Jasak, and C. Fureby, "A tensorial approach to computational continuum mechanics using object-oriented techniques," *Comput. Phys.* **12**, 620–631 (1998).

- ⁴³A. Paszke, S. Gross, F. Massa, A. Lerer, J. Bradbury, G. Chanan, T. Killeen, Z. Lin, N. Gimelshein, L. Antiga *et al.*, “PyTorch: An imperative style, high-performance deep learning library,” *Adv. Neural Inf. Process. Syst.* **32**, 8026–8037 (2019).
- ⁴⁴M. Naumov, M. Arsaev, P. Castonguay, J. Cohen, J. Demouth, J. Eaton, S. Layton, N. Markovskiy, I. Reguly, N. Sakharnykh *et al.*, “AmgX: A library for GPU accelerated algebraic multigrid and preconditioned iterative methods,” *SIAM J. Sci. Comput.* **37**, S602–S626 (2015).
- ⁴⁵R. Collobert, S. Bengio, and J. Mariéthoz, *Torch: A Modular Machine Learning Software Library* (IDIAP, 2002).
- ⁴⁶DeepFlame, <https://github.com/deepmodeling/deepflame-dev>.
- ⁴⁷A. Kazakov and M. Frenklach, <http://www.me.berkeley.edu/drm/>.
- ⁴⁸P. N. Brown, G. D. Byrne, and A. C. Hindmarsh, “Vode: A variable-coefficient ode solver,” *SIAM J. Sci. Stat. Comput.* **10**, 1038–1051 (1989).
- ⁴⁹G. E. Box and D. R. Cox, “An analysis of transformations,” *J. R. Stat. Soc. B* **26**, 211–243 (1964).
- ⁵⁰M. Zhang, Z. An, X. Wei, J. Wang, Z. Huang, and H. Tan, “Emission analysis of the CH₄/NH₃/air co-firing fuels in a model combustor,” *Fuel* **291**, 120135 (2021).
- ⁵¹M. Zhang, X. Wei, J. Wang, Z. Huang, and H. Tan, “The blow-off and transient characteristics of co-firing ammonia/methane fuels in a swirl combustor,” *Proc. Combust. Inst.* **38**, 5181–5190 (2021).
- ⁵²M. Zhang, Z. An, L. Wang, X. Wei, B. Jianayihan, J. Wang, Z. Huang, and H. Tan, “The regulation effect of methane and hydrogen on the emission characteristics of ammonia/air combustion in a model combustor,” *Int. J. Hydrogen Energy* **46**, 21013–21025 (2021).
- ⁵³M. Evans, C. Petre, P. R. Medwell, and A. Parente, “Generalisation of the eddy-dissipation concept for jet flames with low turbulence and low Damköhler number,” *Proc. Combust. Inst.* **37**, 4497–4505 (2019).
- ⁵⁴J. Chomiak and A. Karlsson, “Flame liftoff in diesel sprays,” *Symp. (Int.) Combust.* **26**, 2557–2564 (1996).
- ⁵⁵N. Kornev and E. Hassel, “Method of random spots for generation of synthetic inhomogeneous turbulent fields with prescribed autocorrelation functions,” *Commun. Numer. Meth. Eng.* **23**, 35–43 (2007).
- ⁵⁶F. Proch, P. Domingo, L. Vervisch, and A. M. Kempf, “Flame resolved simulation of a turbulent premixed bluff-body burner experiment. Part I: Analysis of the reaction zone dynamics with tabulated chemistry,” *Combust. Flame* **180**, 321–339 (2017).
- ⁵⁷G. Singh, S. Chander, and A. Ray, “Heat transfer characteristics of natural gas/air swirling flame impinging on a flat surface,” *Exp. Therm. Fluid Sci.* **41**, 165–176 (2012).
- ⁵⁸R. Mao, J. Wang, W. Zhang, Z. An, W. Lin, M. Zhang, and Z. Huang, “Effect of high hydrogen enrichment on the outer-shear-layer flame of confined lean premixed CH₄/H₂/air swirl flames,” *Int. J. Hydrogen Energy* **46**, 17969–17981 (2021).
- ⁵⁹J. Gaucherand, D. Laera, C. Schulze-Netzer, and T. Poinsot, “Intrinsic instabilities of hydrogen and hydrogen/ammonia premixed flames: Influence of equivalence ratio, fuel composition and pressure,” *Combust. Flame* **256**, 112986 (2023).
- ⁶⁰M. S. Sweeney, S. Hochgreb, M. J. Dunn, and R. S. Barlow, “The structure of turbulent stratified and premixed methane/air flames. I: Non-swirling flows,” *Combust. Flame* **159**, 2896–2911 (2012).
- ⁶¹W. Zhang, S. Karaca, J. Wang, Z. Huang, and J. van Oijen, “Large eddy simulation of the Cambridge/Sandia stratified flame with flamelet-generated manifolds: Effects of non-unity Lewis numbers and stretch,” *Combust. Flame* **227**, 106–119 (2021).
- ⁶²X. Qian, C. Zou, H. Lu, and H. Yao, “Large-eddy simulation of Cambridge-Sandia stratified flames under high swirl,” *Combust. Flame* **244**, 112241 (2022).
- ⁶³H. Turkeri, X. Zhao, and M. Muradoglu, “Large eddy simulation/probability density function modeling of turbulent swirling stratified flame series,” *Phys. Fluids* **33**, 025117 (2021).
- ⁶⁴T. Brauner, W. Jones, and A. Marquis, “LES of the Cambridge stratified swirl burner using a sub-grid PDF approach,” *Flow. Turbul. Combust.* **96**, 965–985 (2016).